obtained at multiples of a small fraction of the wavelength in that medium.

Assuming that the dielectric constant of the untreated water is nominally equal to 60, and that this value does not change significantly for small amounts of added salt, then the wavelength of 10 GHz waves propagating though such a medium would be approximately 0.4 cm, so that increases in the path length within the liquid in steps of perhaps 0.04 cm should suffice to detect any existing standing-wave pattern. Inspection of the data for the lower conductivity in Fig. 4 does suggest the presence of a standing wave, but its amplitude is seen to be relatively small compared with the dominant trend of the data.

As mentioned above, the starting medium was chosen to be locally available drinking water "as is." A nonrigorous test or measure of the conductivity of this water may be made by simply immersing both leads of an ohmmeter into the water. In our experiment, using a battery-operated volt-ohm meter (VOM) on the RX1K scale, with the test leads 1 cm apart, the semi quantitative measurement indicated a resistance of approximately 20 kΩ. After the salt was added (20 g per 500 mil of water), the resistance was approximately 4 kΩ.

IV. EXPERIMENTAL RESULTS

Inspection of Fig. 4 indicates that the data points do tend to define a straight line on the semilogarithmic coordinates, indicating that the behavior may be described mathematically by an exponential function with a negative exponent. Moreover, the data indicate that the attenuation is more rapid for the medium with the larger electric conductivity. Inspection of the data for the case of lower conductivity indicates a fairly clear sinusoidal scatter of the data points, suggesting that a noticeable standing wave pattern exists in the medium, and the apparent wavelength appears to be approximately the expected value. Moreover, inspection of the data for the larger conductivity indicates no standing wave pattern, which agrees with the expectation that standing wave patterns in media with higher conductivities will be attenuated progressively more rapidly.

V. CONCLUSION

In reference to the objective in this experiment, which was to verify that in a given lossy medium, the intensity of the propagating electromagnetic wave drops off exponentially with distance traveled in the medium, and that for a given distance traveled the intensity of the wave is a decreasing function of the medium's electric conductivity, it is concluded that the experiment described in this paper does, indeed, achieve this objective.

[1]Further information on the microwave dielectric properties of water is found, for example, in the article by C. W. Kern and M. Karplus, in *The Physics and Physical Chemistry of Water*, edited by Felix Franks (Plenum, New York, 1972), pp. 276ff; J. B. Hastead, *Aqueous Dielectrics* (Chapman and Hall, London, 1973), pp. 43ff. For the purpose of this paper, the microscopic basis for the conductivity of water is not at issue.

[2]J. D. Jackson, *Classical Electrodynamics* (Wiley, New York, 1962), p. 224; P. Lorrain and D. R. Corson, *Electromagnetic Fields and Waves* (Freeman, San Francisco, 1970), Chap. 11; David M. Cook, *The Theory of the Electromagnetic Field* (Prentice Hall, Englewood Cliffs, NJ, 1975), Chap. 13; Arthur F. Kip, *Fundamentals of Electricity and Magnetism* (McGraw-Hill, New York, 1969), Appendix L. Note that our paper follows the treatments presented in the references above inasmuch as the "conductivity" g is being taken in a phenomenological or macroscopic sense.

[3]The static dielectric constant of water at room temperature is given in the literature as approximately 78; this is sometimes called the "low-frequency" value. This value is given, for example, in *Handbook of Chemistry and Physics* (CRC, Boca Raton, FL, 1981), 62nd ed., p. E-58.

Measurement of fluid flow using streak photography

T. D. Dickey, B. Hartman, E. Hurst, and S. Isenogle
Department of Geological Sciences, University of Southern California, Los Angeles, California 90089-0741

(Received 7 February 1983; accepted for publication 8 June 1983)

Streak photography has been used primarily for fluid flow visualizations. A method which extends the application of streak photography to velocity measurements is presented. The technique may be applied to a broad range of fluid dynamical experiments and requires only limited technical resources.

I. INTRODUCTION

Fluid flow problems are currently being studied in the laboratory with a variety of experimental techniques.[1,2] Hot-wire and hot-film anemometry are used primarily in air and water studies, respectively. Both techniques are based upon the principle that changes in fluid velocity can be detected by heated conductivity probes. These methods enable high-frequency (~50 000-Hz) measurements and are ideal for time series analysis. However, relatively complex and expensive data acquisition systems must be employed. In addition, the influence of a probe upon the flow field must be considered. Acoustic and laser anemometry techniques utilize the Doppler effect and enable measurements free of probe disturbances. Unfortunately, these methods are also technically demanding and often cost prohibitive.

Streak photography of a variety of tracer materials (e.g., aluminum flakes, oils, etc.) has been used for qualitative flow visualizations.[1] One major advantage of this method is

that fluid motion with a broad range of scales can be observed throughout a large volume of the fluid. Nonetheless, relatively few investigators have utilized streak photography for quantitative analysis[3–8] because of a lack of acceptable tracer substances, difficulty in determining flow direction, and expensive data reduction. The technique described in this paper has evolved over several years and has overcome these deficiencies.[5,6] Many fluid dynamical experiments may be done with this method which requires relatively modest technical resources.

II. METHOD

The experimental apparatus is shown in Fig. 1. The experimental tank is constructed of 2.5-cm-thick Plexiglas walls and has dimensions of 60 cm × 60 cm × 75 cm. The sides farthest away from the camera and optical system are black because a dark photographic background is required. The experiments are performed in a darkened room and the tank is illuminated with a commercially available mercury vapor lamp of brightness 40 000 cp cm^{-2}. Three 16.5-cm-diam, 22.9-cm focal length low-quality condenser lenses are used to control the tank illumination. The light exposure is controlled by a rotating light chopping wheel with a cutout window. The light beam is interrupted at a pre-set rate which is determined by the voltage applied to a dc motor and is selected to optimize the streaklengths. A piece of Mylar is placed asymmetrically within the window to create photographic streak images consisting of short and long bright sections which are separated by a dim section. Bead direction is thus defined. The exposure time is measured with a simple photodiode and timer circuit. The accuracy is $\pm$ 0.1 ms.

The tracer beads are obtained by sieving a commercially available inert resin (Pliolite VT manufactured by Goodyear Tire and Rubber Company). The size of the beads must be chosen large enough to give adequate light reflection for photography. On the other hand, the time constant for particle motion relative to fluid motion is proportional to the square of the particle diameter.[4] The particle diameter should also be less than the relevant scale of motion.[5,6] A diameter of 0.8 mm is used for the present study although a value of 0.4 mm has been used in previous work in which turbulence has been the focus.[5,6] The frequency response[7,8] of the 0.8-mm beads is approximately 28 Hz and that of the 0.4-mm beads is about 113 Hz. Salt is added to the tank water to achieve a density equal to that of the tracer beads (1.026 g cm^{-3}) and thus buoyancy effects are eliminated.

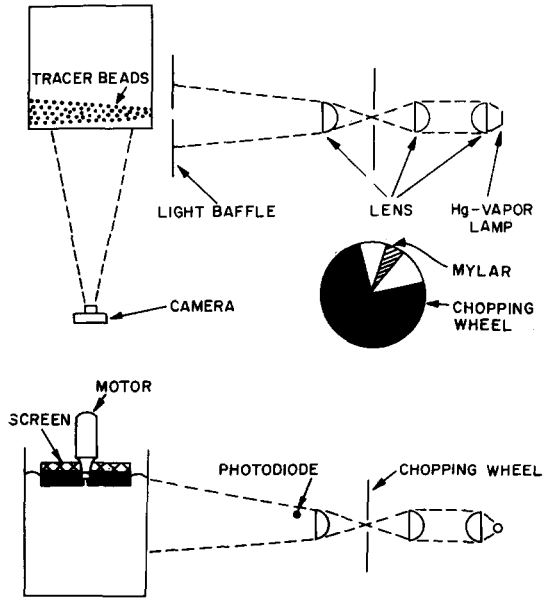

Fig. 1. Schematic diagram of experimental apparatus used to measure fluid flow with streak photography.

A standard 35-mm camera equipped with a zoom lens (80–205 mm) is used to photograph the beads. The shutter control is manually depressed in the bulb mode because light exposure is controlled by the light chopping wheel. Double exposures are not a problem for the range of measurements discussed here. However, if high chopping wheel rotation rates are required, the chopping wheel may be directly synchronized with a motor driven camera using a simple electrical circuit including mechanical trip switches on the chopping wheel and a solenoid to activate the shutter control.[5] The camera is located approximately 2 m from the tank. A standard target board composed of a grid of horizontal and vertical lines spaced at 5-cm intervals is placed in the tank and photographed before each experiment for calibration. The photographic negatives are projected onto the surface of a digitizing pad (graphics tablet) for measurements of target board coordinates and streaklengths. The transformation from digitizing pad distances to *in situ* (tank) distances is given by

$$(\Delta X)_{\text{tank}} = C_x(\Delta X)_{\text{pad}}, \tag{1}$$

$$(\Delta Z)_{\text{tank}} = C_z(\Delta Z)_{\text{pad}}, \tag{2}$$

for the horizonal and vertical displacements, respectively. Distances obtained from the target board grid and the corresponding distances measured with the digitizing pad are used to evaluate constants C_x and C_z. The digitizing system is linked with an RS-232 interface to a computer terminal and computer (a home minicomputer is satisfactory). Target board and streak photographic data are then stored for further processing.

The instantaneous horizontal (x direction) and vertical (z direction) velocity components of each tracer bead (u_j,w_j) are then determined by using calibration constants (C_x,C_z), the exposure time (Δt), and the bead streak endpoint coordinates $(X_H,Z_H)_j$ and $(X_T,Z_T)_j$ which are obtained from the digitizing process. Subscripts H and T refer to the head and tail of the streak from which the direction of movement is established. The horizontal (x direction) and vertical (z direction) velocity components of an individual bead are obtained from the equations

$$u_j = C_x(X_H - X_T)_j/\Delta t, \tag{3}$$

$$w_j = C_z(Z_H - Z_T)_j/\Delta t. \tag{4}$$

III. DISCUSSION

In order to illustrate the method, a simple flow field was established by rotating a screen (driven by an electric motor at 5 rpm) in the upper 2 cm of the water. Before measurements were begun, the fluid was allowed to attain a flow of approximately azimuthal symmetry. Departure from azimuthal flow results from (1) the tank geometry (square versus circular), (2) surging resulting from the rotating screen, and (3) the inherent tank boundary layers (e.g., Ekman

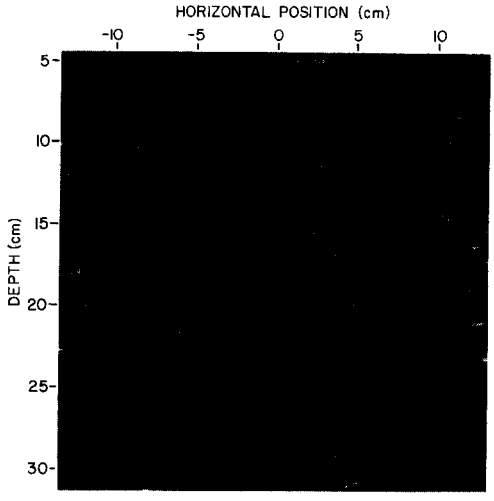

Fig. 2. Streak photograph of neutrally buoyant tracer beads indicating the flow field in the front portion of the tank which is driven by a rotating screen. The bottom of the rotating screen is located approximately 2 cm below the water surface ($z = 0$ cm). The region from approximately 4 to 32 cm below the surface is photographed. The centerline ($x = 0$) bisects the tank.

pumping and side wall effects[9]). A streak photograph of the front portion of the tank (Fig. 2) was digitized. The data were processed as described above. The resulting two-dimensional velocity field is shown in Fig. 3. For illustration, the data obtained from the streak photograph shown in Fig. 2 (along with data from three other streak photographs taken during the same run) were sorted into 14 vertical bins each with vertical extent $\Delta z = 2$ cm. Then ensemble mean velocities were computed for each bin according to

$$\bar{u}(z) = \frac{1}{M}\sum_{j=1}^{M} u_j, \tag{5}$$

$$\bar{w}(z) = \frac{1}{M}\sum_{j=1}^{M} w_j, \tag{6}$$

where M is the number of velocity vectors whose vertical positions fall within a given bin. These profiles are shown in Fig. 4 and indicate that the mean flow in the observed test

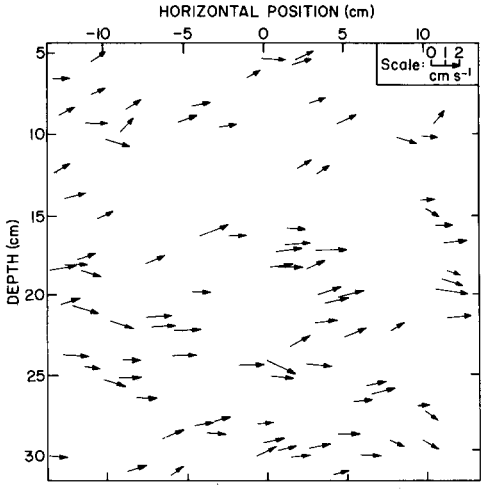

Fig. 3. Computer depiction of the flow field in the front portion of the tank set up by a rotating screen. Data result from the digitized streak photograph of neutrally buoyant beads (Fig. 2) and light exposure time.

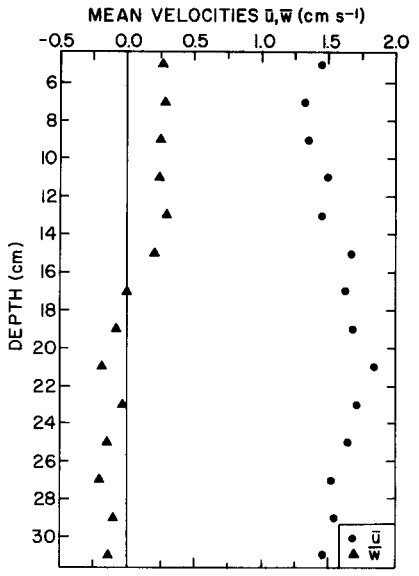

Fig. 4. Depth profiles of mean horizontal velocity $\bar{u}$ and mean vertical velocity $\bar{w}$ in the front portion of the tank obtained from data shown in Fig. 3 and three other streak photographs taken during the same experimental run.

section of the tank was primarily horizontal and approximately uniform with depth. Other portions of the flow field may be studied by simply altering the light baffle position and the optical axis location. Sources of experimental error include: resolution of streak endpoints, exposure time, and calibration constants. The experimental error for the instantaneous velocity measurements was less than $\pm 2\%$.

The present system possesses the following attributes: (1) qualitative and quantitative information may be obtained for relatively large sampling volumes, (2) there are no probe effects, (3) experimental error is comparable to that of other methods, (4) no mean flow is necessary, thus studies of diffusing turbulence can be performed, (5) the apparatus is relatively inexpensive and many components are generally available in physics laboratories, and (6) the data processing may be accomplished with a home mini-computer. Turbulence measurements may be accomplished by decomposing the flow into ensemble mean and fluctuating contributions.[5,6] In addition, a variant of the present technique which uses a stereoscopic optical system[5,6] enables three-dimensional analysis.

ACKNOWLEDGMENTS

This work was supported in part by the National Oceanic and Atmospheric Administration Sea Grant program under grant number NA8/AA-D-00094. Mr. David Morris and co-workers in the USC geology machine shop aided in the design and construction of the experimental apparatus. Special thanks are extended to Michael Lane who expeditiously typed this manuscript.

[1]T. Maxworthy and F. K. Browand, Annu. Rev. Fluid Mech. 7, 273 (1975).
[2]V. A. Sandborn, in *Handbook of Turbulence*, edited by W. Frost and T. H. Moulden (Plenum, New York, 1977), Chap. 11, pp. 321–342.
[3]T. Maxworthy, Phys. Fluids **4**, 558 (1961).
[4]T. Maxworthy, J. Fluid Mech. **93**, 47 (1979).
[5]T. D. Dickey, Ph.D. thesis, Princeton University, 1977.

[6]T. D. Dickey and G. L. Mellor, J. Fluid Mech. **99**, 13 (1980).
[7]A. Fage and H. C. H. Townend, Proc. R. Soc. London, Ser. A **135**, 656 (1932).
[8]W. M. Cady, in *Physical Measurements in Gas Dynamics and Combustion*, edited by R. W. Ladenburg, B. Lewis, R. N. Pease, and H. S. Taylor (Princeton U. P., Princeton, NJ, 1954), pp. 142–158.
[9]J. Pedlosky, *Geophysical Fluid Dynamics* (Springer-Verlag, New York, 1979), pp. 168–235.

On the recurrence phenomenon of a resonant spring pendulum

H. M. Lai
Department of Physics, The Chinese University of Hong Kong, Hong Kong

(Received 13 May 1983; accepted for publication 12 July 1983)

Olsson's coupled equations for a resonant spring pendulum are solved. To-and-fro transfer of energy from one mode to another is shown, the period for such a recurrence is derived, and the patterns of the mass trajectory are obtained. Experimental data are reported and good agreement is found with the theory.

I. INTRODUCTION

When the length and the mass of a spring pendulum are chosen so that the frequency of the spring-type oscillation is twice that of the pendulum-type oscillation, it is long known[1,2] that the motion initially in one mode will change to the other and back and forth. This *resonant* spring pendulum and its "peculiar" behavior has recently attracted much attention[3–8] because it serves as a very good example for demonstrating the phenomena of parametric instability and nonlinear resonant coupling widely studied in nonlinear optics[9] and nonlinear plasma physics.[10]

Theoretically, this is a two-dimensional mechanial problem. Keeping terms up to the third order in the Lagrangian, Minorsky[1] obtained two coupled equations of motion in terms of polar coordinates while Olsson[3] got an *equivalent* but *simpler* set of equations in terms of Cartesian coordinates. They both pointed out that the startup of the sideways pendulum-type mode from the vertical spring-type mode is due to a parametric instability[11] whereas the reverse is due to a resonance effect of the linear type. However, their analysis (and some others'[4]) is restricted to the initial stage of each process and therefore cannot explain the recurrence phenomenon or the to-and-fro transfer of energy from one mode to another. A multiple-time-scale perturbation method has been tried by Falk[6] to account for the recurrence; the correct result was however not obtained due to a serious error in his analysis. Rusbridge[8] has studied Olsson's equations extensively and has also presented experimental and computational results indicating the contribution from higher-order effects. However, he did not obtain enough quantitative results concerning the recurrence phenomenon to make an explicit comparison between theory and experiments. Furthermore, although his equations for the slow-varying amplitudes and phases are correct, the derivation contains an improper assumption.[8]

Nayfeh[12] has also derived the equations for the slow-varying amplitudes and phases from the less-simple formulation in terms of polar coordinates.[1]

In this paper, we solve Olsson's coupled equations of motion through a perturbation method which assumes that the amplitudes and phases of the two oscillating modes are slowly varying. This method is essentially that used by Rusbridge,[8] which turns out to be simpler than the multiple-time-scale perturbation method[13] widely used in solving such problems.[14] Equations for the slow quantities are properly derived. Detailed analysis of these equations shows the to-and-fro transfer of energy from one mode to another. Time variation of the amplitude in terms of an elliptic function is given and the period for the recurrence process is derived. Furthermore, patterns of the mass trajectory or the Lissajou's figures are obtained and their relation to Olsson's observation of stable modes of motion is discussed. In order to test the theory, we have constructed resonant spring pendulums and made measurements on the period of one complete to-and-fro transfer of energy. This is described in Sec. III.

II. ANALYSIS OF THE PROBLEM

We start with Olsson's coupled equations of motion[3]:

$$\ddot{x} + \omega_p^2 x = 3\omega_p^2 xz/L\,, \tag{1}$$

$$\ddot{z} + 4\omega_p^2 z = 3\omega_p^2 x^2/2L\,, \tag{2}$$

where x and z are, respectively, the horizontal and the vertical components of the mass position relative to the equilibrium point, L is the length of the spring (usually plus a

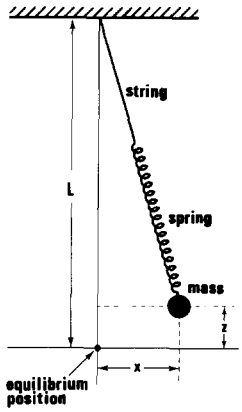

Fig. 1. A spring pendulum.